

A parametric study of Mach reflection in steady flows

By H. LI AND G. BEN-DOR

Pearlstone Center for Aeronautical Engineering Studies, Department of Mechanical Engineering,
Ben-Gurion University of the Negev, Beer Sheva, Israel

(Received 13 May 1996 and in revised form 21 January 1997)

The flow fields associated with Mach reflection wave configurations in steady flows are analysed, and an analytical model for predicting the wave configurations is proposed. It is found that provided the flow field is free of far-field downstream influences, the Mach stem heights are solely determined by the set-up geometry for given incoming-flow Mach numbers. It is shown that the point at which the Mach stem height equals zero is exactly at the von Neumann transition. For some parameters, the flow becomes choked before the Mach stem height approaches zero. It is suggested that the existence of a Mach reflection not only depends on the strength and the orientation of the incident shock wave, as prevails in von Neumann's three-shock theory, but also on the set-up geometry to which the Mach reflection wave configuration is attached. The parameter domain, beyond which the flow gets choked and hence a Mach reflection cannot be established, is calculated. Predictions based on the present model are found to agree well both with experimental and numerical results.

1. Introduction

The phenomenon of shock wave reflection was first mentioned more than one hundred years ago when Mach (1878) experimentally observed two different reflection configurations: regular reflection (RR) and Mach reflection (MR). The study of shock wave reflections was then abandoned for a period of about 70 years until its re-initiation in the early 1940s by von Neumann (1943, 1945) who proposed the two- and three-shock theories for treating RR and MR, respectively. A comprehensive summary of the reflection phenomena can be found in Ben-Dor (1991). Generally, the phenomenon can be divided, depending on whether the flow field under consideration is steady or unsteady, into two categories: stationary and non-stationary reflections. In the present study only stationary reflections are considered.

Schematic illustrations of the wave configurations of RR and MR in steady flows are shown in figures 1(a) and 1(b), respectively. It was pointed out by Emanuel (1986) and Ben-Dor & Takayama (1992) that one of the yet unsolved shock wave reflection problems in steady flows is the mechanism by which the size of a Mach reflection is determined, although several decades have passed since Courant & Friedrichs (1948) and Liepmann & Roshko (1957) raised this problem. In such flows, the height of the Mach stem of a Mach reflection wave configuration is not uniquely determined by von Neumann's three-shock theory. Consider figure 2 where the three solid and one dashed lines describe the four discontinuities of a steady Mach reflection wave configuration, namely the incident (i), the reflected (r) and the Mach stem (m) shock waves, and the slipstream (s). These four discontinuities meet at a single point, the triple point, T. If one selects a new point along the incident shock wave (i) and draws there three lines,

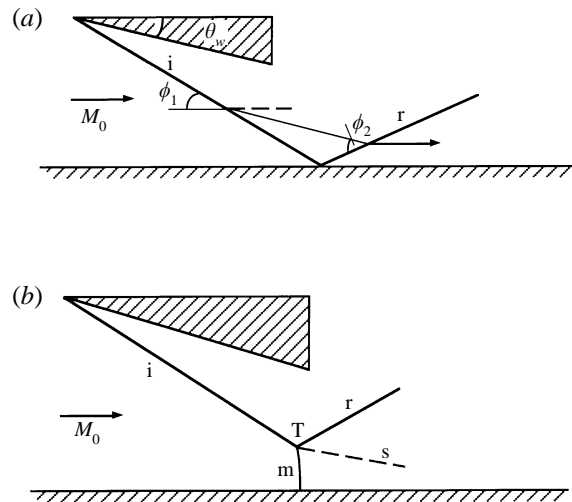


FIGURE 1. Schematic illustration of the wave configuration of (a) regular and (b) Mach reflection in steady flows.

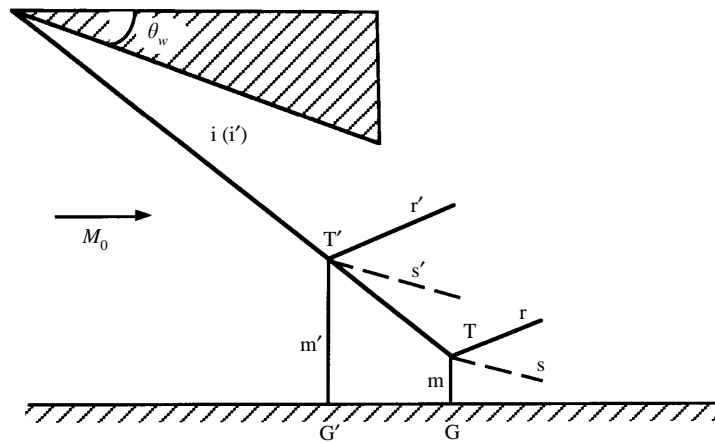


FIGURE 2. Schematic illustration of two theoretically possible Mach reflection wave configurations for identical initial conditions.

one parallel to the reflected shock (r'), one parallel to the Mach stem (m') and one parallel to the slipstream (s') then one has a new triple point, T' , with the appropriate four discontinuities. The two triple points, T and T' , as well as all the other triple points which could have been obtained by choosing a different location for T' along the incident shock wave (i), completely satisfy the governing equations of the three-shock theory of von Neumann (1943, 1945), which, as mentioned earlier, is the basis for the analytical description of a Mach reflection.

However, when experiments with identical initial conditions are repeated in a given facility, only one of the above mentioned infinite theoretically possible Mach reflection wave configurations is obtained. Thus, the three-shock theory is incapable of predicting the actual size of the Mach reflection wave configuration (i.e. Mach stem height) since it is inherently independent of any physical length scale.

There is a need for understanding the mechanism determining the height of the

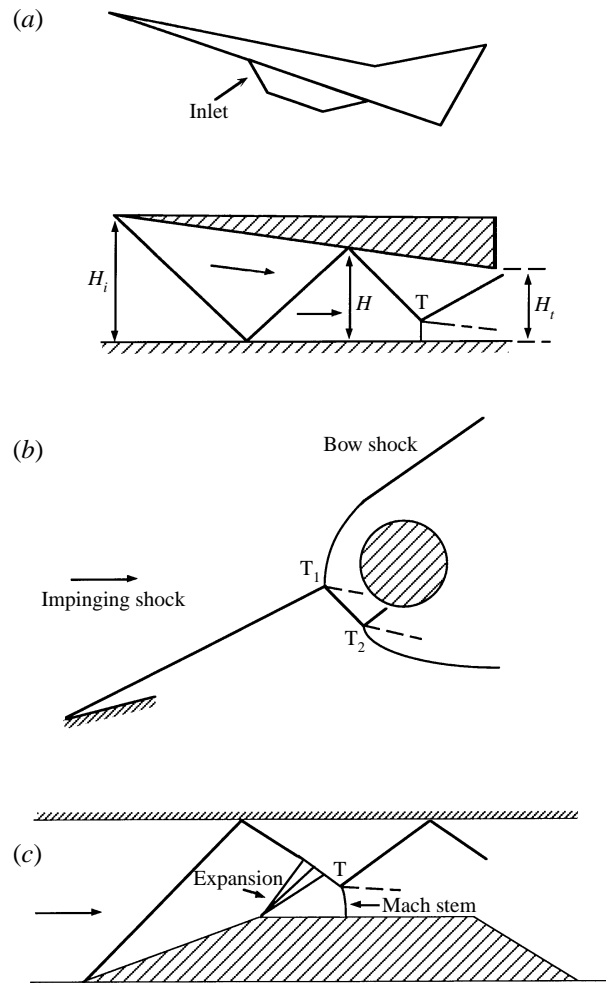


FIGURE 3. Examples of supersonic flows in which a Mach reflection wave configuration actually occurs.

Mach stem, primarily in relation to the design of supersonic vehicles. Figure 3(a) suggests a situation where the length-scale information would be of great importance. It illustrates a simple inlet/combustor configuration for a generic hypersonic craft. An important aspect in the design of such configurations is the variety of internal shock wave patterns which may develop during the flight. Even for the simple inlet geometry shown in figure 3(a) it is apparent that the prevailing shock wave pattern may prevent operation at the desired flight conditions, due to the height of the Mach stem and its effect on the stagnation pressure losses. Indeed, Henderson & Lozzi (1979) contended that the appearance of the Mach stem for certain H_i/H_t ratios is intimately tied to the inlet starting problem.

Figure 3(b) also illustrates a typical interaction, originally investigated by Edney (1968), between an impinging shock and a bow shock. Intense heat transfer to the body surface can occur depending on both the strength and location of the shock waves involved. A key element of certain computational codes currently employed to predict such heating loads is the size of Mach stem shown in the figure. Owing to the lack of an adequate analytical model for predicting the Mach stem size, empirical values have

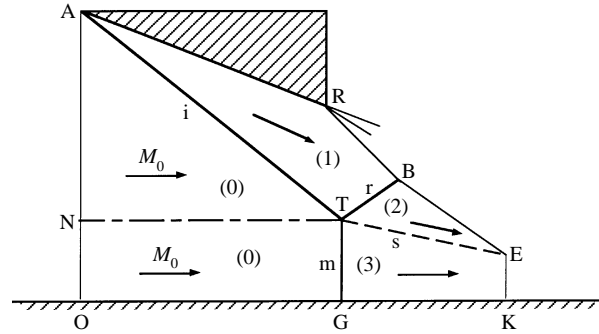


FIGURE 4. Schematic illustration of a Mach reflection wave configuration and definition of a control volume.

been normally utilized. Consequently, it would be a great improvement if estimates of the size of such a Mach stem could be determined solely from the known flow conditions and body geometry.

Similar shock wave patterns may appear in a ram accelerator, which was invented by Hertzberg, Bruckner & Bogdanoff (1988) as a potential new generation of high-speed propulsion devices. The Mach stem, as shown in figure 3(c), plays a key role in the initiation of the detonation downstream. Consequently, the determination of the length of the Mach stem is essential for the design of ram accelerators.

The fact that the flow behind the Mach stem (close to being a normal shock wave) is subsonic leads to yet another reason why the prediction of its height is important. As noted by Back & Cuffel (1971), noise production is greater when subsonic regions exist in otherwise supersonic flows than in a case in which the entire flow field is supersonic. Thus, knowing the extent of such subsonic regions, of which the Mach stem height is a major scaling parameter, may lead to improvements in hardware design based solely on acoustic considerations.

Recently, Azevedo (1989) and Azevedo & Liu (1993) suggested a physical model for predicting the height of the Mach stem. Consider figure 4 where a schematic drawing of a reflecting wedge, which generates a Mach reflection, is shown. In their model they assumed that: (i) the Mach stem is straight; (ii) the slipstream and the bottom surface form an effective one-dimensional converging nozzle; (iii) the throat of this converging nozzle is located at the point where the leading characteristic of the expansion fan (lines RB and BE in figure 4), generated at the trailing edge of the reflecting wedge, intersects the slipstream (point E in figure 4); and (iv) the flow in region (3) is isentropic and reaches sonic conditions at the throat. Then they developed the continuity and the momentum equations as well as some geometric relations for the control volume ARBEKO shown in figure 4. In order to complete the set of the equations, they applied von Neumann's three-shock theory for the triple point T. Since the three-shock theory consists of the continuity, momentum and energy equations across the incident (i), the reflected (r), and the Mach stem (m) shock waves, together with appropriate boundary conditions, the continuity and momentum equations for the control volume ARBETN are used twice if the control volume ARBEKO is divided into two parts, i.e. ARBETN and NTEKO (figure 4). Consequently, the set of the governing equations derived by Azevedo & Liu (1993) could, in fact, be reduced to the control volume NTEKO or TEKG. However, they also applied the quasi-one-dimensional isentropic relation, which actually originates from the continuity and momentum equations for the control volume TEKG, which as mentioned earlier has been used twice. Therefore, there exist

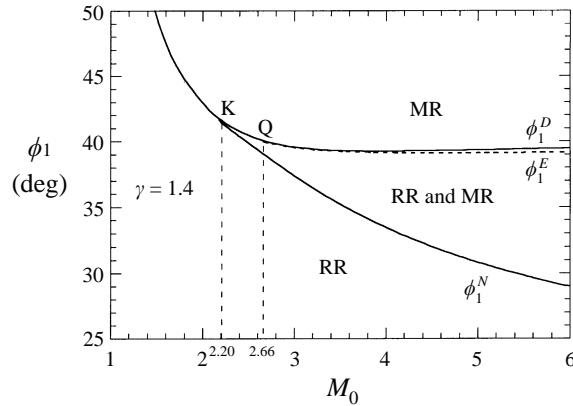


FIGURE 5. Domains of different types of reflections and the transition criteria between them in the (M_0, ϕ_1) -plane.

some doubts in their model equations. This might explain why Azevedo & Liu's (1993) results could not be repeated by using their model equations (A. Chpoun 1995, personal communication). One of the goals of the present study is to propose a realistic model for predicting the Mach stem heights of Mach reflection wave configurations in steady flows.

Another concern of shock wave reflection in steady flows is the transition criterion between regular reflection (RR) and Mach reflection (MR). There are two $RR \leftrightarrow MR$ transition criteria, namely the detachment criterion and the mechanical equilibrium criterion. Both were originally proposed by von Neumann (1943) and the latter reinitiated by Henderson & Lozzi (1975). The transition lines corresponding to these criteria are shown in figure 5 as ϕ_1^D (detachment) and ϕ_1^N (mechanical equilibrium). For $\phi_1 > \phi_1^D$ only MR is theoretically possible while for $\phi_1 < \phi_1^N$ only RR is theoretically possible. In the domain $\phi_1^D > \phi_1 > \phi_1^N$ (which is known as the dual-solution domain) both RR and MR are theoretically possible. Henderson & Lozzi (1975) and Hornung & Robinson (1982), based on their experiments, claimed that the $RR \leftrightarrow MR$ transition takes place at ϕ_1^N . The mechanical equilibrium criterion was accepted by the scientific community as the correct transition criterion. Recently, Li & Ben-Dor (1996a) proved, based on the principle of minimum entropy production, that both RR and MR wave configurations are theoretically stable in the domain $\phi_1^N < \phi_1 < \phi_1^E$, where the line ϕ_1^E is so close to the line ϕ_1^D (the maximum difference is about 0.3°) that they can be practically regarded as the same line. This finding, which contradicted the state of knowledge regarding the transition criterion, was confirmed by Chpoun *et al.*'s (1995) experimental results and Vuillon, Zeitoun & Ben-Dor's (1995) numerical results.

All the transition criteria mentioned above are based on the analysis of local flow fields near the reflection point. They do not account for the set-up geometry to which the shock waves are attached and the influences of the far fields downstream, which have been proved experimentally (Henderson & Lozzi 1979; Hornung & Robinson 1982) to affect the Mach reflection wave configurations as well as their transition to regular reflection. In the present study, we aim at understanding quantitatively how the set-up geometry conditions affect the MR wave configurations, especially their Mach stem size, and their transitions, provided they are free of downstream effects.

2. The present study

2.1. Analysis of the flow field

The half-plane symmetrical MR configuration, usually used in the experiments in order to avoid the viscous boundary wall effects, is shown in figure 6 together with the relevant definition of parameters. Although the symmetrical configuration cannot avoid the viscous boundary-layer growth along the slipstream, s , its influence on the wave configuration is considered to be negligibly small (Azevedo & Liu 1993).

The Mach reflection shown in figure 6 consists of the incident shock (i), the reflected shock (r), the slightly curved Mach stem (m), and the slipstream (s). The flow immediately behind the Mach stem is subsonic. The Mach stem must be perpendicular to the symmetry plane at its foot (point G). The maximum horizontal shift of the foot of the Mach stem is d . The interaction of the reflected shock wave (r), with the centred expansion fan emanating from the trailing edge of the shock-generating wedge results in a transmitted-reflected shock wave (r'), a transmitted expansion fan and an entropy-layer region. More details of the shock wave/expansion fan interaction analysis can be found in Li & Ben-Dor (1996*b*). The transmitted expansion waves strike the slipstream (s) and cause the pressure to drop in the streamwise direction in region (3), thus accelerating the flow to supersonic conditions. As a result, the cross-sectional area of the stream tube between the slipstream (s) and the symmetry plane first decreases to a minimum at a sonic throat (EK in figure 6), and then increases again in the region of the accelerating supersonic flow. A subsonic pocket (TEKG) is therefore formed in an otherwise supersonic flow. The flow downstream of the line RCDEK is supersonic, and hence is isolated from the subsonic pocket. The size and shape of this pocket (eventually the Mach stem height) are solely controlled by the geometry of the upper boundary of region (1) and the distance, H_t , between the trailing edge of the wedge and the symmetry plane.

Hornung & Robinson (1982) correctly pointed out that the normalized Mach stem height, H_m/w , might be expressed as

$$H_m/w = f(\gamma, M_0, \theta_w, H_t/w), \quad (1)$$

where γ , M_0 , θ_w , H_m , H_t and w are the specific heats ratio, the incoming-flow Mach number, the wedge angle, the Mach stem height, the exit cross-sectional area at the trailing edge, and the wedge length, respectively. Unfortunately, they did not give the expression for the function, f . In order to get the analytical expression for determining the size of the Mach stem, one has to solve: (a) the interaction between the reflected shock wave and the expansion fan, (b) the interaction between the transmitted expansion fan and the slipstream, and (c) the flow inside the subsonic pocket. This will be done in §2.2.

The above analysis is based on the assumption that a stable MR wave configuration is well established. One may ask if there are cases (for a given parameter combination of M_0 and θ_w), for which an MR wave configuration is theoretically possible but cannot be established. The answer is yes. This does happen if H_t/w is smaller than a certain value (lower limit) so that the reflected shock wave (r) touches the shock-generating wedge. Consider figure 7, when the reflected shock wave (r) reflects from the wedge surface before it interacts with the expansion fan emanating from the trailing edge, the reflected-reflected shock wave (r') which is formed hits the slipstream (s) at point P. Consequently, either a shock wave or an expansion fan must reflect from the slipstream (s) to match the flow conditions on its other side. Thus a kink should develop at the intersection point, P. Since the flow in region (3) is subsonic, the kink becomes unstable

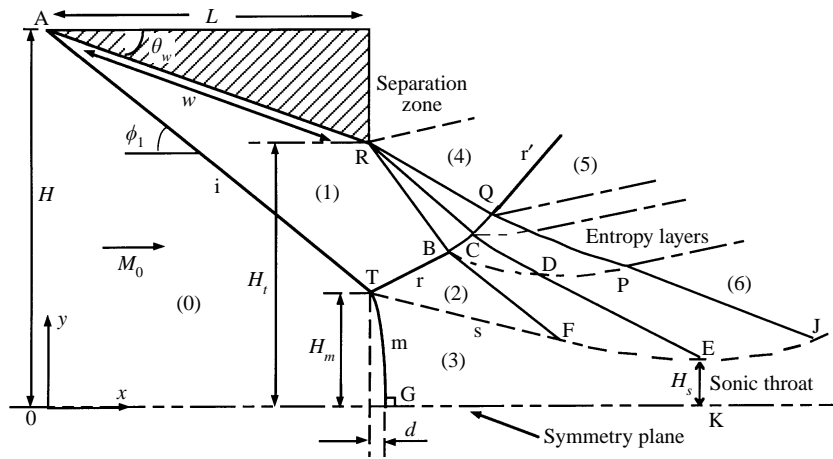


FIGURE 6. Detailed schematic illustration of a Mach reflection wave configuration and definition of relevant parameters.

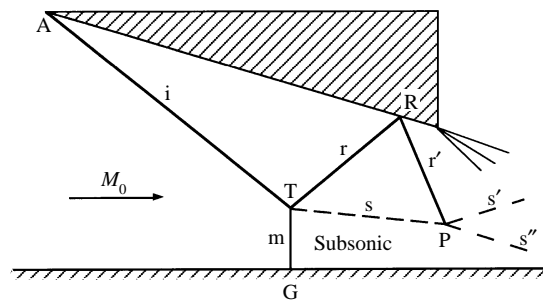


FIGURE 7. Schematic illustration of a possible transient Mach reflection with the reflected shock reflecting as a regular reflection from the wedge surface.

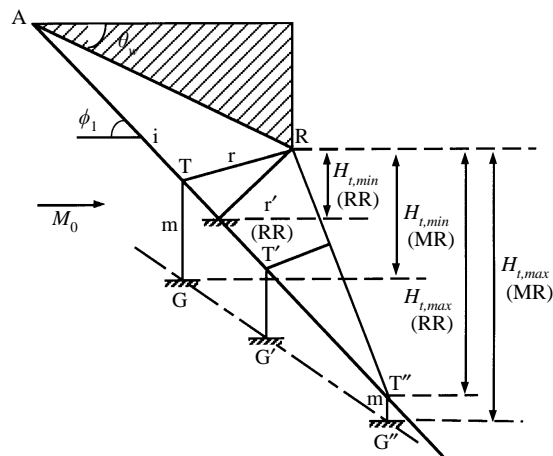


FIGURE 8. Schematic illustration of the limiting cases on the exit cross-sectional area, $H_{t,min}$ and $H_{t,max}$ for both Mach and regular reflection wave configurations.

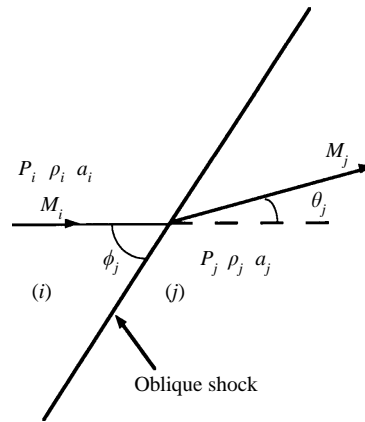


FIGURE 9. Definition of the parameters across an oblique shock wave.

(see Landau & Lifshitz 1987), and the Mach stem is pushed upstream. Finally, the flow gets choked behind the Mach stem reaches the leading edge of the reflecting wedge. This process was observed both in experiments (Chpoun *et al.* 1995) and numerical simulations (Vuillon *et al.* 1995). Therefore, for an MR wave configuration, there exists a minimum value of H_t (lower limit), at which the reflected shock wave grazes the trailing edge. For lower values the flow gets unstated. Consider figure 8: if the combination of M_0 and ϕ_1 is inside the dual-solution domain (see figure 5), an RR wave configuration is also theoretically stable. It is evident from figure 8 that the minimum value of H_t for RR is smaller than that for MR. Unlike an MR wave configuration, an RR wave configuration is still stable when H_t is lower than its minimum value.

There is also an upper limit for which H_t is so large that the leading characteristic of the expansion fan intersects the incident shock wave. The expansion wave then changes both the strength and the orientation of the incident shock. The maximum value of H_t , i.e. $H_{t,max}$, is shown in figure 8. It should be mentioned here that when $H_t > H_{t,max}$, an MR wave configuration may still exist, but its solution is outside the scope of the present study. Based on the foregoing discussion, for a given combination of M_0 , θ_w and w , a Mach reflection will occur provided $H_{t,min}(\text{MR}) < H_t < H_{t,max}(\text{MR})$. The analytical expressions for $H_{t,min}$ and $H_{t,max}$ are given in §3.

2.2. The governing equations

The derivation of the equations is based on the following assumptions: (i) the gas is perfect, and the heat capacities ratio, γ , is constant ($\gamma = 1.4$); (ii) the fluid is ideal, i.e. its dynamic viscosity and thermal conductivity are equal to zero; (iii) the flow in region (2) is supersonic (see figure 6); (iv) the slipstream and the symmetry line form a two-dimensional converging/diverging nozzle. Sonic conditions are reached at the throat (EK in figure 6) of this nozzle provided the flow is free of the far-field downstream influences.

2.2.1. Three-shock-theory solution of the Mach reflection

The well-known three-shock theory (for details see Ben-Dor 1991), can be used to solve the flow field associated with the triple point T of the Mach reflection. Consider figure 9, where an oblique shock wave is schematically drawn together with some relevant flow parameters. The states ahead and behind of the oblique shock wave are (i) and (j), respectively. The angle of incidence is ϕ_j and the flow deflection angle is θ_j .

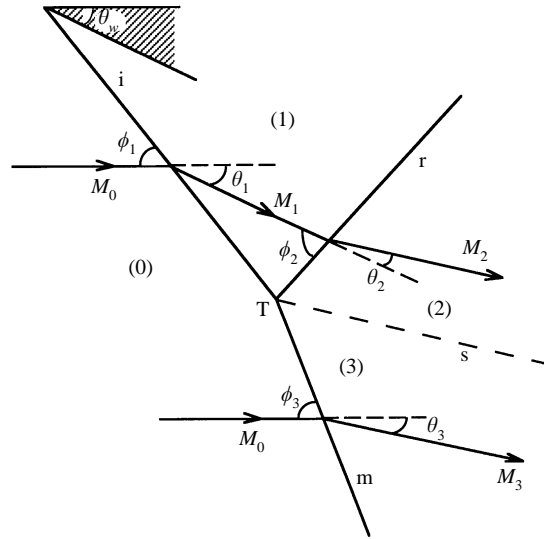


FIGURE 10. Definition of the parameters around the triple point, T.

The flow Mach number is M , the pressure is P , the density is ρ , and the speed of sound is a .

The governing equations of the flow field shown in figure 9 can be combined to read:

$$M_j = F(M_i, \phi_j), \quad \theta_j = G(M_i, \phi_j), \quad P_j = P_i H(M_i, \phi_j), \quad (2a-c)$$

$$\rho_j = \rho_i E(M_i, \phi_j), \quad a_j = a_i A(M_i, \phi_j), \quad (2d, e)$$

where

$$F(M, \phi) = \left\{ \frac{1 + (\gamma - 1) M^2 \sin^2 \phi + \left[\frac{1}{4}(\gamma + 1)^2 - \gamma \sin^2 \phi \right] M^4 \sin^2 \phi}{[\gamma M^2 \sin^2 \phi - \frac{1}{2}(\gamma - 1)] \left[\frac{1}{2}(\gamma - 1) M^2 \sin^2 \phi + 1 \right]} \right\}^{1/2}, \quad (3a)$$

$$G(M, \phi) = \arctan \left[2 \cot \phi \frac{M^2 \sin^2 \phi - 1}{M^2(\gamma + \cos 2\phi) + 2} \right], \quad (3b)$$

$$H(M, \phi) = \frac{2}{\gamma + 1} \left[\gamma M^2 \sin^2 \phi - \frac{1}{2}(\gamma - 1) \right], \quad (3c)$$

$$E(M, \phi) = \frac{(\gamma + 1) M^2 \sin^2 \phi}{(\gamma - 1) M^2 \sin^2 \phi + 2}, \quad (3d)$$

and

$$A(M, \phi) = \frac{[(\gamma - 1) M^2 \sin^2 \phi + 2]^{1/2} [2\gamma M^2 \sin^2 \phi - (\gamma - 1)]^{1/2}}{(\gamma + 1) M \sin \phi}. \quad (3e)$$

Based on the forgoing presentation and the flow parameters which are defined in the schematic illustration of the Mach reflection wave configuration shown in figure 10, the following equations are self-explanatory:

across the incident shock wave (i)

$$M_1 = F(M_0, \phi_1), \quad \theta_1 = G(M_0, \phi_1), \quad P_1 = P_0 H(M_0, \phi_1), \quad (4a-c)$$

$$\rho_1 = \rho_0 E(M_0, \phi_1), \quad a_1 = a_0 A(M_0, \phi_1); \quad (4d, e)$$

across the reflected shock wave (r)

$$M_2 = F(M_1, \phi_2), \quad \theta_2 = G(M_1, \phi_2), \quad P_2 = P_1 H(M_1, \phi_2), \quad (5a-c)$$

$$\rho_2 = \rho_1 E(M_1, \phi_2), \quad a_2 = a_1 A(M_1, \phi_2); \quad (5d, e)$$

across the Mach stem shock (m), near the triple point

$$M_3 = F(M_0, \phi_3), \quad \theta_3 = G(M_0, \phi_3), \quad P_3 = P_0 H(M_0, \phi_3), \quad (6a-c)$$

$$\rho_3 = \rho_0 E(M_0, \phi_3), \quad a_3 = a_0 A(M_0, \phi_3). \quad (6d, e)$$

The boundary conditions are

$$\theta_1 = \theta_w, \quad (7)$$

and across the slipstream s

$$\theta_1 - \theta_2 = \theta_3, \quad (8)$$

$$P_2 = P_3. \quad (9)$$

The above set of equations consist of 18 equations with 18 unknowns, namely $M_1, M_2, M_3, \theta_1, \theta_2, \theta_3, P_1, P_2, P_3, \phi_1, \phi_2, \phi_3, a_1, a_2, a_3, \rho_1, \rho_2$ and ρ_3 , provided the parameters, M_0, P_0, ρ_0 and θ_w are known. Thus, the set of equations is complete and can, in principle, be solved.

Generally, the Mach stem is curved (see figure 6). On the symmetry line at its foot (i.e. at point G), the Mach stem is normal to the upstream flow, M_0 . Consequently, the normal shock relations are valid at point G (i.e. $\phi_G = \pi/2$). They can be written as follows:

$$M_G = F(M_0, \pi/2), \quad P_G = P_0 H(M_0, \pi/2), \quad (10a, b)$$

$$\rho_G = \rho_0 E(M_0, \pi/2), \quad a_G = a_0 A(M_0, \pi/2). \quad (10c, d)$$

The shape of the curved Mach stem is determined by the subsonic flow region behind it. Theoretically, it is impossible to get an exact analytical expression for the shape of the Mach stem. However, based on the experimental fact that the Mach stem is only slightly curved (i.e. the change in the slope of the Mach stem is small), and under the first-order approximation together with the following boundary conditions at points T and G (see definition of parameters in figure 6 as well as the (x, y) -coordinate system chosen)

$$x_T = (H - H_m) \cos \phi_1, \quad (11)$$

$$y_T = H_m, \quad (12)$$

$$(dx/dy)|_T = -\cot \phi_3, \quad (13)$$

$$y_G = 0, \quad (14)$$

and

$$(dx/dy)|_G = 0, \quad (15)$$

the shape of the Mach stem can be expressed as follows (for further details see Appendix A):

$$J_{TG}(x, y) = y^2 \cot \phi_3 + 2H_m x - H_m^2 \cot \phi_3 - 2(H - H_m) H_m \cos \phi_1 = 0, \quad (16)$$

where x_T, y_T, x_G and y_G are the coordinates of the points T and G, respectively, H and H_m , as shown in figure 6, are the distances from the leading edge A and the triple point T to the symmetry line, respectively.

The horizontal shift of the foot of the Mach stem with respect to the triple points is

$$d = x_G - x_T = \frac{1}{2} H_m \cot \phi_3. \quad (17)$$

The only unknown parameter in equations (11)–(17) is the height of the Mach stem, H_m .

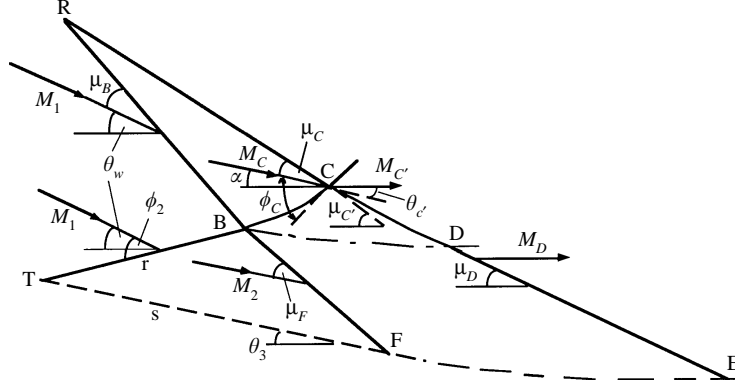


FIGURE 11. Schematic illustration of the interaction of the expansion fan with the reflected shock wave (r) and slipstream (s) and definition of the relevant parameters.

2.2.2. Interaction of the expansion fan with the reflected shock wave and the slipstream

The interaction of the centred expansion fan with the reflected shock wave, r, is shown schematically in figures 6 and 11 in which the relevant flow parameters are also defined. Based on the flow field analysis in §2.1, the Mach reflection wave configuration does not depend on the flow parameters in the regions downstream of the line RCDE (see figure 6) provided it is free of downstream influences. Consequently, only the governing equations for solving the relevant flow regions shown in figure 1 are needed.

The region RBC is a Prandtl–Meyer fan, therefore

$$\nu(M_C) - \nu(M_1) = \theta_w - \alpha, \quad (18)$$

$$P_C = P_1 \left[\frac{2 + (\gamma - 1) M_1^2}{2 + (\gamma - 1) M_C^2} \right]^{\gamma/(\gamma - 1)}, \quad (19)$$

where M_C and P_C are the flow Mach number and the pressure along the characteristic RC, α is the flow direction relative to the horizontal direction, and $\nu(M)$ is the Prandtl–Meyer function, i.e.,

$$\nu(M) = \left(\frac{\gamma + 1}{\gamma - 1} \right)^{1/2} \arctan \left[\frac{(\gamma - 1)(M^2 - 1)}{\gamma + 1} \right]^{1/2} - \arctan (M^2 - 1)^{1/2}. \quad (20)$$

Across the curved shock wave at point C, one gets

$$M_{C'} = F(M_C, \phi_C), \quad \theta_{C'} = G(M_C, \phi_C), \quad P_{C'} = P_C H(M_C, \phi_C), \quad (21a-c)$$

where $M_{C'}$, $\theta_{C'}$ and $P_{C'}$ are the flow Mach number, the flow deflection angle and the pressure immediately behind the curved reflected shock at point C, respectively.

The interaction of the expansion fan with the reflected shock wave results in an entropy-layer region (see figure 6). The dashed-dotted line BDP is a weak tangent discontinuity. The region BQP, which is not a simple wave region, is filled with an infinity of such entropy layers. The pressure and the flow direction remain the same across each entropy layer while the entropy, the density and the other thermodynamic properties change in infinitesimal increments. Therefore, the overall changes of the flow properties across the entire entropy layers region result in a situation in which the flow directions at points C and D along curve CD are parallel and the pressures are the same, i.e.

$$\alpha = \theta_{C'}, \quad (22)$$

$$P_{C'} = P_D, \quad (23)$$

where P_D is the pressure at point D. It should be noted here that had $P_{C'}$ been different from P_D a steady entropy layer, such as the one separating regions (5) and (6), could not exist, in contrast to available experimental results.

When the transmitted expansion waves reach the slipstream (s), they partially reflect from it and partially transmit through it. As analysed in Appendix B under the first-order approximation, the reflected expansion waves are very weak and hence can be neglected. Thus, region BFED (see figure 6) can be assumed to be a simple wave region. Consequently, the flow parameters along the lines BF and DE remain constant. At point E where the sonic throat is located, the flow direction should be parallel to the x -axis. Again by using the Prandtl–Meyer relation one gets

$$\nu(M_D) - \nu(M_2) = \theta_3, \quad (24)$$

$$P_D = P_2 \left[\frac{2 + (\gamma - 1) M_2^2}{2 + (\gamma - 1) M_D^2} \right]^{\gamma/(\gamma-1)}. \quad (25)$$

The above set of equations (18)–(25) consists of nine equations with nine unknowns, i.e. M_C , $M_{C'}$, M_D , P_C , $P_{C'}$, P_D , ϕ_C , θ_C and α . Consequently, it is complete provided all the other parameters are known, as indeed is the case.

2.2.3. Flow through the subsonic pocket (region TEKG in figure 6)

The flow in the duct formed by the slipstream and the symmetry line (TE and GK, respectively, in figure 6) is subsonic. Theoretically, it is impossible to get an exact analytical solution in this subsonic flow region. However, for the cases under consideration the Mach stem is only slightly curved and generally $\theta_3 \ll 1$. Consequently, it is reasonable to assume that the flow in the duct TEKG is quasi-one-dimensional. As assumed earlier, the flow isentropically becomes sonic at the throat (EK in figure 6). The well known quasi-one-dimensional area–Mach number relation results in

$$\frac{H_m}{H_s} = \frac{1}{\bar{M}} \left[\frac{2}{\gamma+1} \left(1 + \frac{\gamma-1}{2} \bar{M}^2 \right) \right]^{\gamma+1/(2(\gamma-1))}. \quad (26)$$

Here, \bar{M} can be regarded as the average flow Mach number behind the curved Mach stem. It is defined as

$$\bar{M} = \bar{u}/\bar{a}, \quad (27)$$

where under a first-order approximation

$$\bar{u} = \frac{1}{H_m \bar{\rho}} \int_0^{H_m} \rho \mathbf{u} \cdot \mathbf{e}_x \, dy = \frac{1}{2\bar{\rho}} (\rho_3 u_3 \cos \theta_3 + \rho_G u_G), \quad (28a)$$

$$\bar{a} = \frac{1}{2}(a_3 + a_G), \quad \bar{\rho} = \frac{1}{2}(\rho_3 + \rho_G). \quad (28b, c)$$

Substituting equations (28a) to (28c) into (27) results in

$$\bar{M} = \frac{2(\rho_3 u_3 \cos \theta_3 + \rho_G u_G)}{(\rho_3 + \rho_G)(a_3 + a_G)}, \quad (29)$$

where $u_3 = M_3 a_3$ and $u_G = M_G a_G$, u_3 , M_3 , ρ_3 and θ_3 can be obtained from the solution of equations (4) to (9) and M_G , ρ_G and a_G are given by equations (10a), (10c) and (10d).

Recall that the Mach stem height H_m is still unknown in the above set of equations, the geometric relations of the wave configuration, given by equation (C11) in Appendix C, provide the required extra equation to close this set of equations.

It should be pointed out here that the actual flow in the pocket TEKG is two-dimensional, and hence the flow parameters are not uniform in the cross-sections of the pocket, i.e. along the y -axis (see figure 6). This can be seen clearly in the numerical simulations of Chpoun *et al.* (1994) and Ivanov, Gimelshein & Beylich (1995). Under the quasi-one-dimensional flow assumption, the average flow parameters in the cross-sections are used in the related equations. Inspecting the matching conditions across the slipstream indicates that the pressures in region (2), where flow is supersonic and uniform (TF is a straight line), and in the region downstream of the expansion wave region, are not necessarily equal to the average pressure in the pocket. But the flow directions on the two sides of the slipstream at the sonic throat (EK) where the minimum cross-section area is reached, are the same and parallel to the x -axis direction. The three-shock-theory solution (equations (4) to (9)) is valid only in the regions near the triple point T. The matching condition across the slipstream at point E is the flow directions (equation (24)) rather than the pressures.

3. Results and discussion

The governing equations derived in §2 were solved by MATLAB. Among the calculated parameters, the most interesting one is the Mach stem height for the given appropriate initial conditions. A comparison between the normalized Mach stem height H_m/L as predicted based on the model developed here (solid line) and as observed by Hornung & Robinson (1982) (solid squares) is shown in figures 12(a) and 12(b) for $M_0 = 2.84$ and 3.98, respectively. The geometry condition is $H_t/L = 0.37$. In addition, Azevedo & Liu's (1993) calculated results (dashed line) and Vuillon *et al.*'s (1995) numerical results (open circles) are added to these figures. It is evident that when compared with both the experimental and the numerical results, the present predictions are better than those of Azevedo & Liu (1993). Furthermore, the Mach stem heights based on the present prediction approach zero exactly at the von Neumann transition point, ϕ_1^N . This indicates that the MR \rightarrow RR transition takes place at the von Neumann criterion. Note that Azevedo & Liu's (1993) predicted transition angle is greater than the von Neumann transition angle (see figures 12a and 12b). This inconsistency may come from the earlier mentioned contradiction in the governing equations of their model.

The predicted values of the Mach stem heights are slightly lower than the experimental data and the numerical simulations for larger values of M_0 (see figure 12b). In spite of the fact that the assumptions used for the present model might introduce errors to some extent, the main reason may be attributed to the experimental uncertainty and the numerical code used. This can be seen in tables 1 and 2 where results of more cases are presented and compared. An inspection of table 1 indicates that for the same value of M_0 with slightly different geometrical conditions, the present analytical results can be larger or smaller than the experimental data. The dependence of H_m/H on the geometrical parameters is very sensitive, especially when the Mach stem height is small. Comparisons between numerical predictions of different codes and the analytical results for the same value of $M_0 = 4.96$ with different geometrical conditions are shown in table 2. Depending on the numerical code, the numerical simulated results can be either larger or smaller than the analytical predictions.

As analysed in §2.1, an MR wave configuration is well established only when the geometrical set-up to which the MR is attached satisfies the condition that $H_{t,min}(\text{MR}) < H_t < H_{t,max}(\text{MR})$, where $H_{t,max}(\text{MR})$ and $H_{t,min}(\text{MR})$ are the upper and the lower limits of H_t , respectively. They can be easily calculated from the parameters given in figures 6, 8 and 11 as

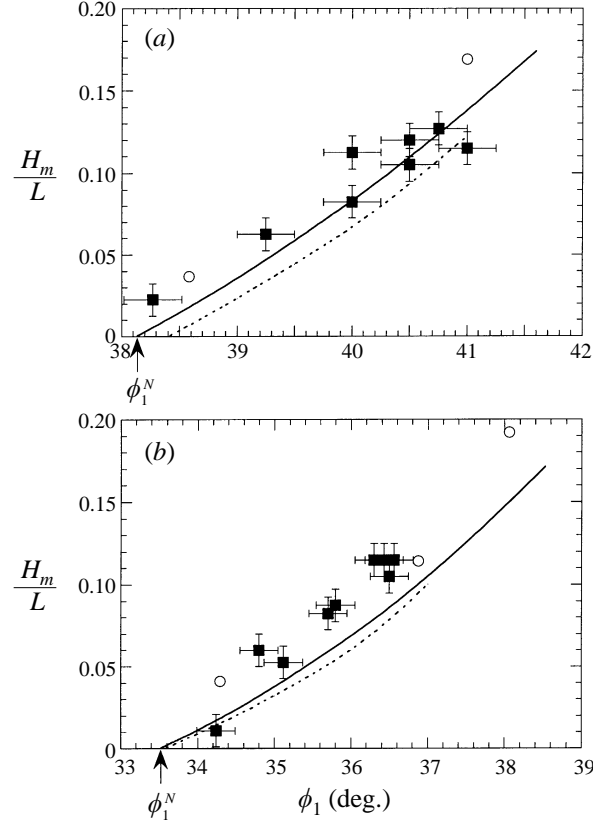


FIGURE 12. Comparisons of the analytically predicted normalized Mach stem height, with experimental (Hornung & Robinson 1982, solid squares) and numerical (Vuillon *et al.* 1995, circles) results for $H_t/L = 0.37$. Dashed line, Azevedo & Liu's calculated results. (a) $M_0 = 2.84$, and (b) $M_0 = 3.98$.

Case	M_0	ϕ_1 (deg)	w/H	H_m/H	
				Experimental	Analytical
1	2.84	$40 \pm .03$	1.42	0.14 ± 0.01	0.11
2	2.84	40.7 ± 0.3	1.48	0.15 ± 0.01	0.17
3	4.96	32 ± 0.3	1.39	0.037 ± 0.005	0.028
4	4.96	32 ± 0.3	1.40	0.013 ± 0.005	0.017

TABLE 1. Comparison of the non-dimensional Mach stem height, H_m/H , between the experimental results of Hornung (1979, personal communication) and Hornung & Robinson's (1982) and the present analytical predictions

$$H_{t,max}(\text{MR}) = H_m + \frac{w \sin(\mu_B + \theta_w) \sin(\phi_1 - \theta_w)}{\sin(\mu_B + \theta_w - \phi_1)} \quad (30)$$

and

$$H_{t,min}(\text{MR}) = H_m + \frac{w \sin(\phi_2 - \theta_w) \sin(\phi_1 - \theta_w)}{\sin(\phi_1 + \phi_2 - \theta_w)}. \quad (31)$$

If the (M_0, ϕ_1) -combination is in the domain where both MR and RR are theoretically possible, i.e. $\phi_1^N < \phi_1 < \phi_1^E \approx \phi_1^D$ (see figure 5), a stable RR wave

Case	θ_w (deg)	w/H	H_m/H			
			Numerical ¹	Numerical ²	Numerical ³	Analytical
1	30	0.77	0.23	—	—	0.21
2	32	0.77	0.33	—	—	0.35
3	27.5	1.25	—	0.24	—	0.28
4	27.8	1.25	—	0.28	—	0.31
5	26.9	1.1	—	—	0.20	0.19
6	28	1.1	—	—	0.27	0.27

¹ Chpoun *et al.*'s (1994) numerical results based on a finite volume zonal code.

² Ivanov *et al.*'s (1995) numerical results based on a DSMC code.

³ Shirozu & Nishida's (1995) numerical results based on a TVD code.

TABLE 2. Comparison of the non-dimensional Mach stem height between numerical results and the present analytical predictions for $M_0 = 4.96$ with different geometrical set-up parameters

configuration is also possible. For an RR wave configuration, the upper and lower limits of H_t can be calculated in a similar way as

$$H_{t,max}(\text{RR}) = \frac{w \sin(\mu_B + \theta_w) \sin(\phi_1 - \theta_w)}{\sin(\mu_B + \theta_w - \phi_1)} \quad (32)$$

and

$$H_{t,min}(\text{RR}) = \frac{w \sin(\phi_2 - \theta_w) \sin(\phi_1 - \theta_w)}{\sin(\phi_1 + \phi_2 - \theta_w)}. \quad (33)$$

It should be noted here that in (32) and (33) ϕ_2 is calculated from a regular reflection (see figure 1) and is, of course, larger than the ϕ_2 in MR for the same values of M_0 and θ_w . It can be seen in figure 8 that $H_{t,max}(\text{RR}) < H_{t,max}(\text{MR})$ and that $H_{t,min}(\text{RR}) < H_{t,min}(\text{MR})$. It is very important to note that an RR wave configuration is still stable when its reflected shock wave reaches the reflecting wedge surface, i.e. $H_t(\text{RR}) < H_{t,min}(\text{RR})$, since the mechanism which causes the MR wave configuration to become unstable when $H_t(\text{MR}) < H_{t,min}(\text{MR})$ (recall the analysis in §2.1) does not exist in the case of an RR. In the following text, for simplicity $H_{t,max}$ and $H_{t,min}$ will be used to refer to $H_{t,max}(\text{MR})$ and $H_{t,min}(\text{MR})$, respectively, since the limiting values of an MR are more important.

Vuillon *et al.* (1995), based on their numerical simulations, introduced the MR \rightarrow RR transition value of H_t , $H_{t,tr}$, at the condition where $H_m = 0$. They found that for some given parameters $H_{t,min} < H_{t,tr} < H_{t,max}$ (see figure 13). Consequently, they concluded that ‘in the range $H_{t,min} < H_t < H_{t,tr}$ the stable wave configurations were Mach reflections and in the range $H_{t,tr} < H_t < H_{t,max}$ the stable wave configurations were regular reflections. Regular reflection wave configurations, which were established in the range $H_{t,min} < H_t < H_{t,tr}$ were found to be unstable’. Furthermore, they stated that their ‘numerical attempts to establish Mach reflection wave configurations in the range $H_{t,tr} < H_t < H_{t,max}$ failed’. But Vuillon *et al.* (1995) mistakenly calculated the values of $H_{t,max}$ based on their incorrect equation (6) which is only valid when $H_m = 0$ (which actually does not occur). A comparison between the different calculations for $H_{t,max}$ are shown in table 3. As can be seen, the values of $H_{t,max}$ calculated here are smaller than those calculated mistakenly by Vuillon *et al.* (1995). It is evident that for all cases $H_{t,max} < H_{t,tr}$. Therefore, $H_{t,tr}$ does not exist at all because the incident shock wave will be caught by the expansion fan generated from the trailing edge before the

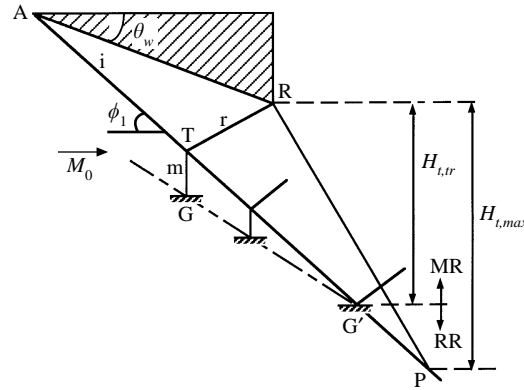


FIGURE 13. Schematic illustration of the MR ↔ RR transition at $H_{t,min} < H_{t,tr} < H_{t,max}$ as proposed by Vuillon *et al.* (1995).

Case	M_0	θ_w (deg)	$H_{t,tr}$ (cm)	$H_{t,max}$ (cm)		
				Incorrect ¹	Correct ²	Present ³
1	3.98	23.6	5.85	7.85	5.49	5.74
2	4.96	26.56	5.65	5.90	4.67	5.25
3	4.96	25.0	5.05	5.70	4.65	4.95
4	6.0	26.56	4.85	5.15	4.14	4.66
5	7.0	26.56	4.65	5.10	3.82	4.34

¹ The values cited here were mistakenly calculated by Vuillon *et al.* (1995) based on equation (6) in their paper.

² The correctly calculated results are based on the same equation (6) in Vuillon *et al.*'s (1995) paper.

³ The calculated results are based on equation (30) in the present study.

TABLE 3. Comparison of the numerically determined values of $H_{t,tr}$ (Vuillon *et al.* 1995) with the values of $H_{t,max}$ calculated by different models. The wedge length, w , is 7 cm

condition $H_m \rightarrow 0$ is reached for any given parameter combination (M_0, ϕ_1) in the dual-solution domain. Consequently, Vuillon *et al.*'s (1995) conclusion cited above is incorrect.

The dependence of the normalized upper and lower limits, $H_{t,max}/w$ and $H_{t,min}/w$, on ϕ_1 is shown in figure 14. The normalization factor is the wedge length, w , which is usually a fixed value in a supersonic vehicle design or in wind tunnel experiments. The two vertical dashed lines refer to the two transition positions ($\phi_1^N = 30.9^\circ$ and $\phi_1^D = 39.3^\circ$), and the two horizontal dashed-dotted lines are the upper and lower limit values of H_t for an RR wave configuration. An MR wave configuration can exist only in the domain between the two solid lines. The flow becomes unstated if the parameters (H_t and ϕ_1) lie in the domain below the line corresponding to $H_{t,min}$. This is a key element in the design of ramjet engine.

The calculated Mach stem heights and locations for $M_0 = 4.96$ and $\theta_w = 25^\circ$ (which correspond to a point inside dual-solution domain) for a fixed value of w (assigned to be unity) is shown in figure 15. It can be seen that the Mach stem height decreases monotonically as H_t increases, and reaches maximum and minimum values at $H_t =$

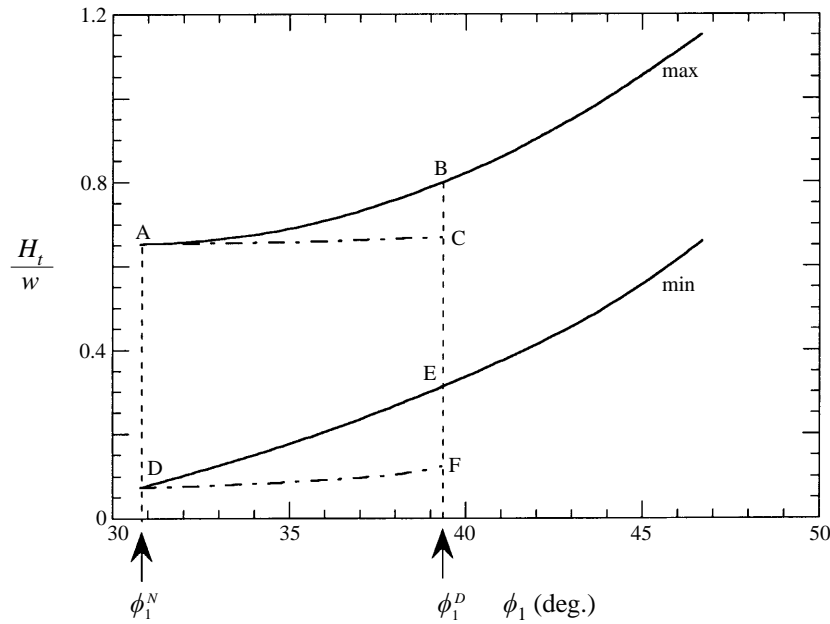


FIGURE 14. Dependence of the normalized upper and lower limiting values of H_t , $H_{t,max}/w$ and $H_{t,min}/w$, on the incident shock wave angle ϕ_1 and domains where regular and Mach reflection wave configurations are either stable or unstable. $M_0 = 5$.

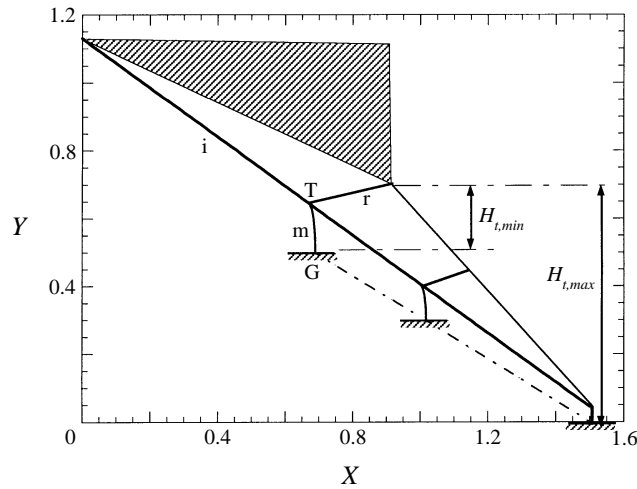


FIGURE 15. Analytical prediction of the shape and location of a Mach reflection wave configuration in the domain $H_{t,min} < H_t < H_{t,max}$ for a fixed wedge length $w = 1$. $M_0 = 4.96$, $\theta_w = 25^\circ$.

$H_{t,min}$ and $H_t = H_{t,max}$, respectively. The calculation did verify that an MR \rightarrow RR transition does not take place in the range $H_{t,min} < H_t < H_{t,max}$. This contradicts Vuillon *et al.*'s (1995) numerical results (case 3 in their paper). The calculations also indicated that within the forth-order approximation the trajectory of the Mach stem foot (point G) is a straight line. This finding is yet to be explained.

An almost linear dependence of the ratio of the maximum shift of the Mach stem

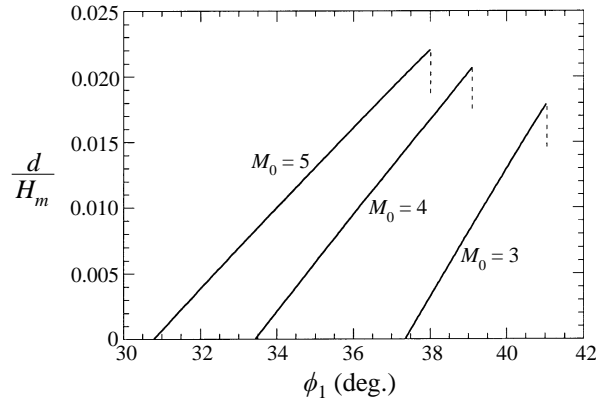


FIGURE 16. Dependence of the normalized horizontal shift of Mach stem, d/H_m , on the incident shock wave angle ϕ_1 for different values of flow Mach number M_0 . $w/H = 1.4$.

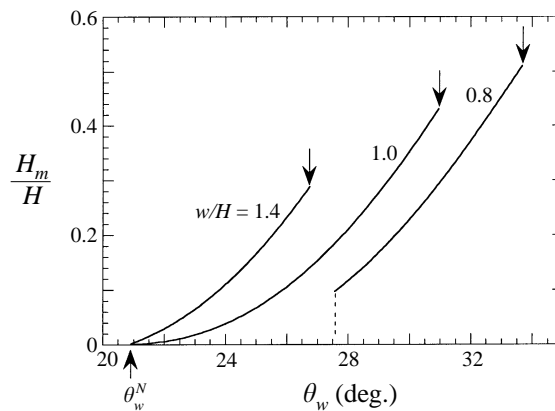


FIGURE 17. Dependence of the normalized Mach stem height, H_m/H , on the reflecting wedge angle θ_w for different values of normalized wedge length w/H with the upper and the lower limits (arrows). $M_0 = 5$.

to the Mach stem height, d/H_m , on ϕ_1 is evident in figure 16 for $M_0 = 3, 4$ and 5 and $w/H = 1.4$. The maximum value of d/H_m is about 0.02 , which means that the curvatures of the Mach stem are very small. This is consistent with experimental observations. This fact can explain why many investigators who assumed straight Mach stems did not introduce pronounced errors, although the Mach stems are theoretically not straight. (Note that the straight Mach stem can be theoretically obtained only at $\phi_1 = \phi_1^N$, but under such a condition, according to the present model, there is no Mach stem since $H_m = 0$.)

The dependence of H_m/H on θ_w for $M_0 = 5$ and different geometrical ratios is shown in figure 17. For the cases $w/H = 1.4$ and 1.0 , the Mach stem heights reach zero smoothly, with different slopes, at the von Neumann point. A. Chpoun (1995, personal communication) experimentally observed the same phenomenon. But for the case $w/H = 0.8$ (see dashed line), the Mach stem height cannot approach zero. Instead, it reaches its minimum value $H_m/H = 0.1$, beyond which H_t becomes greater than $H_{t,max}$. In all the above three cases, the Mach stem heights have maximum values, indicated by arrows.

Finally, a Mach reflection wave configuration for $M_0 = 5$ and $\theta_w = 28^\circ$ with a

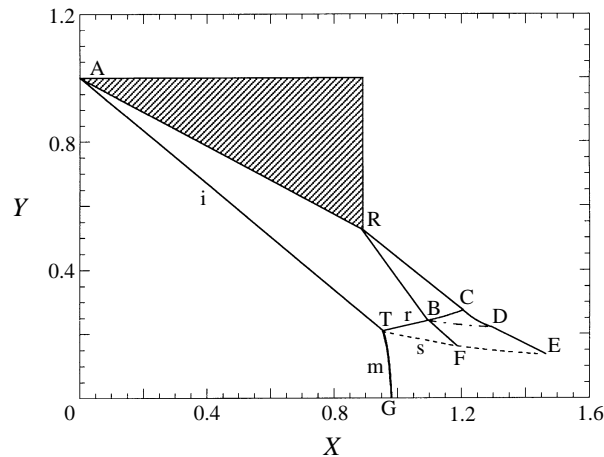


FIGURE 18. Analytical prediction of a Mach reflection wave configuration for $M_0 = 5$, $\theta_w = 28^\circ$ and $H = 1$.

detailed wave configuration, which was calculated using the present model, is shown in figure 18. It is evident that the interaction between the expansion fan emanating from the trailing edge and the reflected shock wave (r), as well as the slipstream (s), results in a curved part of the shock wave (BC), a curved part of the characteristic (CD) and a curved part of the slipstream (FE). The sonic throat (point E) is located downstream of point F where the first characteristic intersects the slipstream. Recall that Azevedo & Liu's (1993) model was based on the assumption that the sonic throat is located at point F. Obviously this is not the case. The mechanism by which the expansion fan centred at the trailing edge of the reflecting wedge creates the sonic throat and carries information on the upper geometrical conditions through the subsonic pocket to the Mach stem, and hence determines its size and location is self-explanatory. This was initially noted by Sternberg (1959) and later by Hornung, Oertel & Sandeman (1979). In the present study, however, for the first time, the quantitative relations describing this mechanism are presented.

It should be mentioned here that the foregoing results and discussion were based on the assumption that the MR wave configuration was isolated from downstream influences. Under some circumstance, downstream influences can not be ignored. Usually, the downstream influences could be a result of higher or lower pressures imposed at the far field downstream. The Mach stem height can either increase or decrease in the presence of such influences. Henderson & Lozzi (1979) and Hornung & Robinson (1982) experimentally observed that the Mach stem height became greater by introducing higher downstream pressures. A physical mechanism for such a process is not clear as yet. This should be subject of further study.

4. Conclusions

The Mach reflection wave configurations as well as the resulting flow field in steady flows were analysed and formulated. The governing equations were derived based on the assumptions that the flow is inviscid and free of downstream influences. A physical mechanism by which the centred expansion fan creates the sonic throat and hence determines the Mach stem height was quantitatively described. It was found that for given incoming-flow Mach numbers the Mach stem heights are solely determined by

the geometrical set-up. It was shown that the point at which the Mach stem height reached zero was exactly at the von Neumann transition condition. For some parameters, the flow became choked before the Mach stem height reached zero. It was suggested that the existence of a Mach reflection did not depend only on the strength and orientation of the incident shock wave, as postulated by von Neumann's three-shock theory, but also on the geometrical set-up to which the Mach reflection was attached. The parameter domains for which the flow became unstated and hence a Mach reflection could not be established were calculated. Predictions based on the present model were found to agree well with both experimental and numerical results.

It is believed that the analytical model developed in the present study identifies the dominant factors that affect the size and location of Mach reflection wave configurations in certain steady flow situations. The present work was intended to complement the relatively large effort devoted to shock reflections in pseudo-steady and unsteady flows, as well as to provide a basis for more complete steady-flow models. The model developed here can be also used to validate the numerical codes dealing with similar problems.

We acknowledge support for this research by the Israel Science Foundation, under grant no. 173/95.

Appendix A. Derivation of a general expression for a curved line as a function of some boundary conditions at its ends

A monotonic curve $Q_1 Q_2$ is shown in figure 19. The coordinates of the points Q_1 and Q_2 in the (x, y) -coordinate system are (x_1, y_1) and (x_2, y_2) , respectively. The slopes at points Q_1 and Q_2 are $\tan \delta_1$ and $\tan \delta_2$, respectively. If the curve $Q_1 Q_2$ satisfies the condition that $\delta_2 - \delta_1 = \delta \ll 1$, its analytical expression can be obtained under the first-order approximation provided the appropriate parameters are known. The derivation is given in the following.

The transformation from the (x, y) - to the (x', y') -coordinate system is (see figure 19)

$$x' = (x - x_1) \cos \delta_1 + (y - y_1) \sin \delta_1, \quad (\text{A } 1 \text{ a})$$

$$y' = -(x - x_1) \sin \delta_1 + (y - y_1) \cos \delta_1. \quad (\text{A } 1 \text{ b})$$

The coordinates of the points Q_1 and Q_2 in the (x', y') -coordinate system are $(0, 0)$ and (x'_2, y'_2) , respectively. The slopes at points Q_1 and Q_2 are 0 and $\tan(\delta_2 - \delta_1)$, respectively.

By assuming that $\tan(\delta_2 - \delta_1) = \epsilon$, where $\epsilon \ll 1$, one can get the following equation for the curve $Q_1 Q_2$:

$$y' = f(x') < \epsilon x' \leq \epsilon x'_2. \quad (\text{A } 2)$$

For the case under study, the curve $Q_1 Q_2$ is either BC, CD, BD or EF (see figure 6). $x'_2 < 1$ is always valid if the maximum characteristic length is taken as the normalization factor. Then, by using Taylor expansion equation (A 2) becomes

$$y' = f(x') = f(0) + f'_{x'}(0)x' + \frac{1}{2}f''_{x'x'}(0)(x')^2 + o(\epsilon). \quad (\text{A } 3)$$

Since at point Q_1 , $y' = 0$ and $dy'/dx' = 0$, and at point Q_2 , $dy'/dx' = \epsilon$, one finally gets

$$y' = f(x') = \frac{(x')^2}{2x'_2} \epsilon, \quad (\text{A } 4)$$

which at point Q_2 yields

$$y'_2 = \frac{1}{2}x'_2 \epsilon. \quad (\text{A } 5)$$

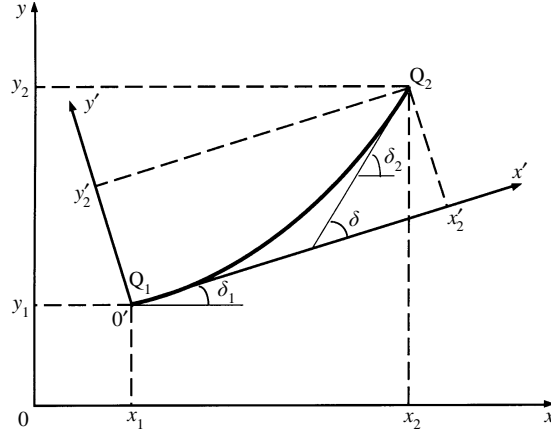


FIGURE 19. Schematic illustration of a monotonic curve and definition of relevant parameters in both (x, y) - and (x', y') -coordinates.

Returning to the (x, y) -coordinate system, the following expressions for the curve $Q_1 Q_2$ can be obtained by substituting (A 1a) and (A 1b) into (A 4) and (A 5):

$$J(x, y, x_1, y_1, x_2, y_2, \delta_1, \delta_2) = [(y - y_1) \tan \delta_1 + (x - x_1)]^2 \tan(\delta_2 - \delta_1) + 2[(x_2 - x_1) + (y_2 - y_1) \tan \delta_1][(x - x_1) \tan \delta_1 - (y - y_1)] = 0 \quad (\text{A } 6)$$

$$\text{and} \quad y_2 - y_1 = \tan A(\delta_1, \delta_2)(x_2 - x_1), \quad (\text{A } 7)$$

$$\text{where} \quad A(\delta_1, \delta_2) = \arctan \left[\frac{2 \tan \delta_1 + \tan(\delta_2 - \delta_1)}{2 - \tan \delta_1 \tan(\delta_2 - \delta_1)} \right]. \quad (\text{A } 8)$$

Equation (A 6) is a general expression for a curved line as a function of some boundary conditions at its ends.

Appendix B. Estimation of the strength of the expansion waves which are reflected at the slipstream

When an incident wave collides head-on with a gas interface, it can partially reflect from and partially transmit through the interface (see figure 20). The reflection coefficient, R , can be defined as

$$R = \frac{|1 - Z_i/Z_t|}{|1 + Z_i/Z_t|}, \quad (\text{B } 1)$$

where Z_i and Z_t are the wave impedances of states (i) and (t) at the acoustic limit, respectively, i.e. $Z_i = \rho_i a_i$ and $Z_t = \rho_t a_t$ (for details, see Henderson 1989). The intensity reflection coefficient, R_I , is

$$R_I = R^2 |Z_i/Z_r|, \quad (\text{B } 2)$$

where Z_r is the wave impedance of state (r) at the acoustic limit, i.e. $Z_r = \rho_r a_r$. When the incident wave is an expansion wave, which is the case under study, Z_r approximately equals Z_i . Therefore, (B 2) can be simplified to read

$$R_I = R^2 = \frac{|\rho_t a_t - \rho_i a_i|^2}{|\rho_t a_t + \rho_i a_i|^2}. \quad (\text{B } 3)$$

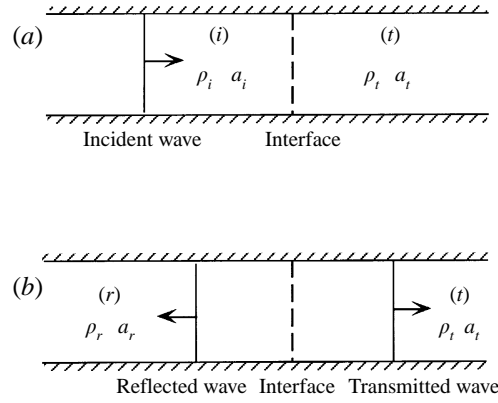


FIGURE 20. Schematic illustration of the head-on interaction of a wave with a gas interface. (a) Prior to the interaction; (b) after the interaction.

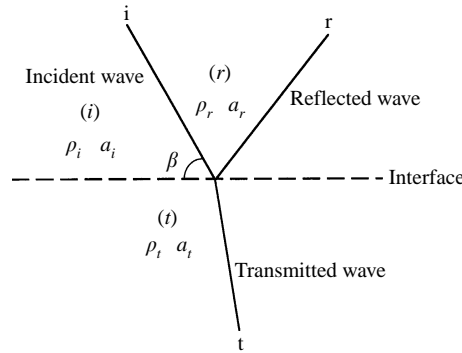


FIGURE 21. Schematic illustration of the oblique interaction of an expansion wave with a gas interface.

If the incident expansion wave impacts the gas interface obliquely (see figure 21), the intensity reflection coefficient is

$$R_I = R^2 \cos^2 \beta = \left| \frac{\rho_t a_t - \rho_i a_i}{\rho_t a_t + \rho_i a_i} \right|^2 \cos^2 \beta. \quad (\text{B } 4)$$

In the case under study, i.e. the gas interface is the slipstream separating the flow regions (2) and (3), $\rho_i a_i = \rho_2 a_2$ and $\rho_t a_t = \rho_3 a_3$. For any (M_0, θ_w) combination of an MR, based on the three-shock-theory calculations (equations (4)–(9)), the following inequality is always valid:

$$\left| \frac{\rho_3 a_3 - \rho_2 a_2}{\rho_3 a_3 + \rho_2 a_2} \right| < 0.2. \quad (\text{B } 5)$$

By combining (B 4) and (B 5), one obtains the intensity reflection coefficient of the expansion wave from region (2) shown in figure 6 as

$$R_I = \left| \frac{\rho_3 a_3 - \rho_2 a_2}{\rho_3 a_3 + \rho_2 a_2} \right|^2 \cos^2 \beta \leq \left| \frac{\rho_3 a_3 - \rho_2 a_2}{\rho_3 a_3 + \rho_2 a_2} \right|^2 < 0.04. \quad (\text{B } 6)$$

Therefore, under the first-order approximation the reflected wave from the slipstream (see figure 6) is negligibly small and hence can be neglected.

Appendix C. Geometric relations for the wave configuration shown in figures 6 and 11

The coordinates of the relevant intersection points shown in figure 6 are assigned to be $R(x_R, y_R)$, $B(x_B, y_B)$, $C(x_C, y_C)$, $D(x_D, y_D)$, $E(x_E, y_E)$ and $F(x_F, y_F)$:

for the straight line RB (see figure 11),

$$y_B - y_R = -\tan(\mu_B + \theta_w)(x_B - x_R), \quad (\text{C } 1a)$$

where

$$\mu_B = \arcsin(1/M_1), \quad x_R = L = w \cos \theta_w, \quad y_R = H - w \sin \theta_w; \quad (\text{C } 1b-d)$$

for the straight line RC (see figure 11)

$$y_C - y_R = -\tan(\mu_C + \alpha)(x_C - x_R), \quad (\text{C } 2a)$$

where

$$\mu_C = \arcsin(1/M_C); \quad (\text{C } 2b)$$

for the straight line BF (see figure 11)

$$y_F - y_B = -\tan(\mu_F + \theta_3)(x_F - x_B), \quad (\text{C } 3a)$$

where

$$y_F = H_s, \quad \mu_F = \arcsin(1/M_2); \quad (\text{C } 3b, c)$$

for the straight line DE (see figure 11)

$$y_E - y_D = -\tan \mu_D(x_E - x_D), \quad (\text{C } 4a)$$

where

$$\mu_D = \arcsin(1/M_D); \quad (\text{C } 4b)$$

for the straight line TB (see figure 11)

$$y_B - y_T = \tan(\phi_2 - \theta_w)(x_B - x_T), \quad (\text{C } 5a)$$

where

$$y_T = H_m, \quad x_T = (H - H_m) \cos \phi_1; \quad (\text{C } 5b, c)$$

and for the straight line TF (see figure 11)

$$y_F - y_T = -\tan \theta_3(x_F - x_T). \quad (\text{C } 6)$$

The exact analytical expressions for the curved lines BC, CD, BD and FE are hard to obtain. But an inspection of the formation of these lines, which result from the interaction of the expansion waves (weak discontinuities) with the shock wave, slipstream and tangent weak discontinuities, indicates that their slopes are only slowly changing and the total variations are small. Under the first-order approximation, their analytical expression can be obtained using the procedure presented in Appendix A.

The expression for the curved line BC (see figure 11) is

$$J[x, y, x_B, y_B, x_C, y_C, \delta_B(\text{BC}), \delta_C(\text{BC})] = 0, \quad (\text{C } 7a)$$

and

$$y_B - y_C = \tan A[\delta_B(\text{BC}), \delta_C(\text{BC})](x_B - x_C), \quad (\text{C } 7b)$$

where $\delta_B(\text{BC})$ and $\delta_C(\text{BC})$ are the angles of inclination of the curve BC at points B and C, respectively, which are given by

$$\delta_B(\text{BC}) = \phi_2 - \theta_w, \quad \delta_C(\text{BC}) = \phi_C - \alpha, \quad (\text{C } 7c, d)$$

and the functions J and A are given by (A 5) and (A 7) in Appendix A, respectively.

For the curved line CD (see figure 11), one gets

$$J[x, y, x_C, y_C, x_D, y_D, \delta_C(\text{CD}), \delta_D(\text{CD})] = 0 \quad (\text{C } 8a)$$

and
$$y_C - y_D = \tan A[\delta_C(\text{CD}), \delta_D(\text{CD})](x_C - x_D), \quad (\text{C } 8b)$$

where $\delta_C(\text{CD})$ and $\delta_D(\text{CD})$ are the angles of inclination of the curve CD at points C and D, respectively, which are given by

$$\delta_C(\text{CD}) = -\mu_{C'} = -\arcsin(1/M_{C'}), \quad \delta_D(\text{CD}) = -\mu_D = -\arcsin(1/M_D). \quad (\text{C } 8c, d)$$

For the curved line BD (see figure 11), one gets

$$J[x, y, x_B, y_B, x_D, y_D, \delta_B(\text{BD}), \delta_D(\text{BD})] = 0 \quad (\text{C } 9a)$$

and
$$y_B - y_D = \tan A[\delta_B(\text{BD}), \delta_D(\text{BD})](x_B - x_D), \quad (\text{C } 9b)$$

where $\delta_B(\text{BD})$ and $\delta_D(\text{BD})$ are the angles of inclination of the curve BD at points B and D, respectively, which are given by

$$\delta_B(\text{BD}) = \theta_3, \quad \delta_D(\text{BD}) = 0. \quad (\text{C } 9c, d)$$

For the curved line FE (see figure 11), one gets

$$J[x, y, x_F, y_F, x_E, y_E, \delta_F(\text{FE}), \delta_E(\text{FE})] = 0 \quad (\text{C } 10a)$$

and
$$y_F - y_E = \tan A[\delta_F(\text{FE}), \delta_E(\text{FE})](x_F - x_E), \quad (\text{C } 10b)$$

where $\delta_F(\text{FE})$ and $\delta_E(\text{FE})$ are the angles of inclination of the curve FE at points F and E, respectively, which are given by

$$\delta_F(\text{FE}) = -\theta_3, \quad \delta_E(\text{FE}) = 0. \quad (\text{C } 10c, d)$$

By combining (C 1 a) to (C 10 d) one finally gets the following expression relating the parameters H_m and H_s :

$$H_m = R(H_s, H, w, \theta_w, \phi_2, \theta_3, \alpha, M_1, M_2, M_C, M_{C'}, M_D). \quad (\text{C } 11)$$

REFERENCES

- AZEVEDO, D. J. 1989 Analytical prediction of shock patterns in a high-speed wedge bounded duct. PhD thesis, Dept. Mech. & Aero. Engng, State University NY, Buffalo.
- AZEVEDO, D. J. & LIU, C. S. 1993 Engineering approach to the prediction of shock patterns in bounded high-speed flows. *AIAA J.* **31**, 83–90.
- BACK, L. H. & CUFFEL, R. F. 1971 Viscous slipstream flow downstream of a centerline Mach reflection. *AIAA J.* **9**, 2107–2109.
- BEN-DOR, G. 1991 *Shock Wave Reflection Phenomena*. Springer.
- BEN-DOR, G. & TAKAYAMA, K. 1992 The phenomena of shock wave reflection – a review of unsolved problems and future research needs. *Shock Waves* **2**, 211–223.
- CHPOUN, A., PASSEREL, D., LENGAND, J. C., LI, H. & BEN-DOR, G. 1994 Mise en évidence expérimentale et numérique d'un phénomène d'hystérésis lors de la transition réflexion de Mach-réflexion régulière. *C. R. Acad. Sci. Paris* **319**, II, 1447–1453.
- CHPOUN, A., PASSEREL, D., LI, H. & BEN-DOR, G. 1995 Reconsideration of oblique shock wave reflection in steady flows. Part 1. Experimental investigation. *J. Fluid Mech.* **301**, 19–35.
- COURANT, R. & FRIEDRICHS, K. O. 1948 *Supersonic Flow and Shock Waves*. Wiley-Interscience.
- EDNEY, B. E. 1968 Effects of shock impingement on the heat transfer around blunt bodies. *AIAA J.* **6**, 15–21.
- EMANUEL, G. 1986 *Gasdynamics: Theory and Applications*. AIAA.
- HENDERSON, L. F. 1989 On the refraction of shock waves. *J. Fluid Mech.* **198**, 365–386.
- HENDERSON, L. F. & LOZZI, A. 1975 Experiments on transition of Mach reflection. *J. Fluid Mech.* **68**, 139–155.
- HENDERSON, L. F. & LOZZI, A. 1979 Further experiments on transition of Mach reflection. *J. Fluid Mech.* **94**, 541–539.

- HERTZBERG, A., BRUCKNER, A. P. & BOGDANOFF, D. W. 1988 Ram accelerator: a new chemical method for accelerating projectiles to ultrahigh velocities. *AIAA J.* **26**, 195–203.
- HORNUNG, H. G., OERTEL, H. & SANDEMAN, R. J. 1979 Transition to Mach reflection of shock waves in steady and pseudo-steady flow with and without relaxation. *J. Fluid Mech.* **90**, 541–560.
- HORNUNG, H. G. & ROBINSON, M. L. 1982 Transition from regular to Mach reflection of shock waves. Part 2. The steady-flow criterion. *J. Fluid Mech.* **123**, 155–164.
- IVANOV, M. S., GIMELSHEIN, S. F. & BEYLICH, A. E. 1995 Hysteresis effect in stationary reflection of shock waves. *Phys. Fluids* **7**, 685–687.
- LANDAU, L. D. & LIFSHITZ, E. M. 1987 *Fluid Mechanics*. Pergamon.
- LI, H. & BEN-DOR, G. 1996*a* Application of the principle of minimum entropy production to shock wave reflections. Part I. Steady flows. *J. Appl. Phys.* **80**, 2027–2037.
- LI, H. & BEN-DOR, G. 1996*b* Oblique-shock/expansion-fan interactions: analytical solution. *AIAA J.* **34**, 418–421.
- LIEPMANN, H. W. & ROSHKO, A. 1957 *Elements of Gasdynamics*. John Wiley & Sons.
- MACH, E. 1878 Uber den Verlauf von Funkenwellen in der Ebene und im Raume. *Sitzungsbr Akad Wiss Wien* **78**, 819–838.
- NEUMANN, J., VON 1943 Oblique reflection of shock. *Explos. Res. Rep.* 12. Navy Dept., Bureau of Ordinance, Washington, DC. (also *Collected Works*, vol. 6, pp. 238–299, Pergamon).
- NEUMANN, J., VON 1945 Refraction, Intersection and Reflection of Shock Waves. *NAVORD Rep.* 203–45. Navy Dept., Bureau of Ordinance, Washington, DC.
- SHIROZU, T. & NISHIDA, M. 1995 Numerical studies of oblique shock reflection in steady two-dimensional flows. *Memoirs Faculty Engng, Kyushu Univ.* **55**, 193–204.
- STERNBERG, J. 1959 Triple shock-wave intersections. *Phys. Fluids* **2**, 178–206.
- VUILLON, J., ZEITOUN, D. & BEN-DOR, G. 1995 Reconsideration of oblique shock wave reflection in steady flows. Part 2. Numerical investigation. *J. Fluid Mech.* **301**, 37–50.